

1 **Reviewing Global Estimates of Surface Reactive Nitrogen Concentration and**
2 **Deposition Using Satellite Retrievals**

3 Lei Liu ^{a,*}, Xiuying Zhang ^b, Wen Xu ^c, Xuejun Liu ^c, Xuehe Lu ^b, Jing Wei ^{d,e}, Yi Li ^f,
4 Yuyu Yang ^a, Zhen Wang ^b, Anthony Y. H. Wong ^g

5 ^a College of Earth and Environmental Sciences, Lanzhou University, Lanzhou 730000,
6 China

7 ^b International Institute for Earth System Science, Nanjing University, Nanjing,
8 210023, China

9 ^c College of Resources and Environmental Sciences, National Academy of
10 Agriculture Green Development, China Agricultural University, Beijing, 100193,
11 China

12 ^d State Key Laboratory of Remote Sensing Science, College of Global Change and
13 Earth System Science, Beijing Normal University, Beijing, China

14 ^e Department of Atmospheric and Oceanic Science, Earth System Science
15 Interdisciplinary Center, University of Maryland, College Park, MD, USA

16 ^f Chief Technology Officer SailBri Cooper Inc., Beaverton OR, 97008, USA

17 ^g Department of Earth and Environment, Boston University, Boston, MA 02215, USA

18 * Correspondence to Lei Liu (liuleigeo@lzu.edu.cn).

19 **Abstract**

20 Since the industrial revolution, human activities have dramatically changed the
21 nitrogen (N) cycle in natural systems. Anthropogenic emissions of reactive nitrogen
22 (N_r) can return to the earth's surface through atmospheric N_r deposition. Increased N_r
23 deposition may improve ecosystem productivity. However, excessive N_r deposition
24 can cause a series of negative effects on ecosystem health, biodiversity, soil, and
25 water. Thus, accurate estimations of N_r deposition are necessary for evaluating its

26 environmental impacts. The United States, Canada and Europe have successively
27 launched a number of satellites with sensors that allow retrieval of atmospheric NO₂
28 and NH₃ column density, and therefore estimation of surface N_r concentration and
29 deposition at an unprecedented spatiotemporal scale. Atmosphere NH₃ column can be
30 retrieved from atmospheric infra-red emission, while atmospheric NO₂ column can be
31 retrieved from reflected solar radiation. In recent years, scientists attempted to
32 estimate surface N_r concentration and deposition using satellite retrieval of
33 atmospheric NO₂ and NH₃ columns. In this study, we give a thorough review on
34 recent advances of estimating surface N_r concentration and deposition using the
35 satellite retrievals of NO₂ and NH₃, present a framework of using satellite data to
36 estimate surface N_r concentration and deposition based on recent works, and
37 summarize the existing challenges for estimating surface N_r concentration and
38 deposition using the satellite-based methods. We believe that exploiting satellite data
39 to estimate N_r deposition has a broad and promising prospect.

40 **Keywords**

41 Nitrogen deposition; Satellite retrieval; Surface concentration; Oxidized and reduced
42 N_r

43 **1. Introduction**

44 Nitrogen (N) exists in three forms in the environment including reactive nitrogen (N_r),
45 organic nitrogen (ON) and nitrogen gas (N₂) (Canfield et al., 2010). N₂ is the main
46 component of air, accounting for 78% of the total volume of air, but it cannot be
47 directly used by most plants. N_r refers to the general term of N-containing substances
48 in atmosphere, plants, soils and fertilizers that are not combined with carbon. N_r (such
49 as NO₃⁻ and NH₄⁺) is the main form of N that can be directly used by most plants, but
50 the content of N_r in nature is much lower compared with ON and N₂ (Vitousek et al.,

51 1997;Nicolas and Galloway, 2008). The supply of N_r is essential for all life forms and
52 contributes to the increase in agricultural production, thus providing sufficient food
53 for the growing global population (Galloway et al., 2008;David et al., 2013;Galloway
54 et al., 2004b;Erisman et al., 2008). Before the industrial revolution, N_r mainly came
55 from natural sources such as biological N fixation, lightning and volcanic eruption
56 (Galloway et al., 2004a). Since the industrial revolution, human activities (e.g.
57 agricultural development, combustion of fossil energy) have greatly perturbed the N
58 cycle in natural systems (Canfield et al., 2010;Kim et al., 2014;Lamarque et al.,
59 2005).

60 N_r (NO_x and NH_3) emitted to the atmosphere will return to the earth surface through
61 atmospheric deposition (Liu et al., 2011). Atmospheric N_r deposition refers to the
62 process in which N_r are removed from the atmosphere, including wet (rain and snow)
63 and dry (gravitational settling, atmospheric turbulence, etc.) deposition (Xu et al.,
64 2015;Zhang et al., 2012;Pan et al., 2012). The input of N_r over terrestrial natural
65 ecosystems primarily comes from the N_r deposition (Shen et al., 2013;Sutton et al.,
66 2001;Larssen et al., 2011). In the short term, atmospheric N_r deposition can increase
67 the N_r input to ecosystems, which promotes plant growth and enhances ecosystem
68 productivity (Erisman et al., 2008;Sutton et al., 2013). However, excessive
69 atmospheric N_r deposition also causes a series of environmental problems (Liu et al.,
70 2017d). Due to the low efficiency of agricultural N application, plenty of N_r is lost
71 through runoff, leaching and volatilization, causing serious environmental pollution.
72 Excessive N_r deposition may aggravate the plant's susceptibility to drought or frost,
73 reduce the resistance of plant to pathogens or pests, and further affect the physiology
74 and biomass distribution of vegetation (ratio of roots, stems and leaves) (Stevens et al.,
75 2004;Nadelhoffer et al., 1999;Bobbink et al., 2010;Janssens et al., 2010). Excessive

76 N_r leads to eutrophication and related algal blooms over aquatic ecosystems, reducing
77 water biodiversity (Paerl et al., 2014), while excessive N_r in drinking water also poses
78 a threat to human health (Zhao et al., 2013). Therefore, monitoring and estimation of
79 surface N_r concentration and deposition on the global scale are of great importance
80 and urgency.

81 The methods of estimating atmospheric N_r deposition can be divided into three
82 categories: ground-based monitoring, atmospheric chemical transport modeling
83 (ACTM) and satellite-based estimation. Ground-based monitoring is considered to be
84 the most accurate and quantitative method, which can effectively reflect the N_r
85 deposition in local areas. ACTM can simulate the processes of N_r chemical reaction,
86 transport, and deposition, as well as the vertical distribution of N_r . Satellite-based
87 estimation establishes empirical, physical or semi-empirical models by connecting the
88 ground-based N_r concentrations and deposition with satellite-derived N_r concentration.
89 This study focuses on reviewing the recent development of satellite-based methods to
90 estimate N_r deposition. We firstly give a brief introduction to the progress of
91 ground-based monitoring, ACTM-based methods, and then present a detailed
92 framework of using satellite observation to estimate dry and wet N_r deposition
93 (including both oxidized and reduced N_r). Next, we review the recent advances of the
94 satellite-based methods of estimating N_r deposition. Finally, we discuss the remaining
95 challenges for estimating surface N_r concentration and deposition using satellite
96 observation.

97 **2 Methods for Estimating Surface N_r Concentration and Deposition**

98 **2.1 Ground-based Monitoring**

99 Ground-based monitoring of N_r deposition can be divided into two parts: wet and dry
100 N_r deposition monitoring. Since the 1970s, there have been large-scale monitoring

101 networks focusing on the wet N_r deposition. The main large-scale regional monitoring
102 networks include Canadian Air and Precipitation Monitoring Network (CAPMoN),
103 Acid Deposition Monitoring Network in East Asia (EANET), European Monitoring
104 and Evaluation Program (EMEP), United States National Atmospheric Deposition
105 Program (NADP), World Meteorological Organization Global Atmosphere Watch
106 Precipitation Chemistry Program, and Nationwide Nitrogen Deposition Monitoring
107 Network in China (NNDMN) (Tan et al., 2018; Vet et al., 2014). The detailed
108 scientific objectives of the wet N_r deposition observation networks vary, but most of
109 the observation networks mainly concentrate on the spatiotemporal variation of wet
110 deposition of ions including N_r compounds, the long-term trends of ions in
111 precipitation, and the evaluation of ACTMs.

112 Compared with wet N_r deposition monitoring, dry N_r deposition monitoring started
113 late, due to the limitation of monitoring technology since it is more difficult to be
114 quantified (affected greatly by surface roughness, air humidity, climate and other
115 environmental factors) (Liu et al., 2017c). Dry N_r deposition observation networks
116 include US ammonia monitoring network (AMoN), CAPMoN, EANET and EMEP.
117 The monitoring methods of dry N_r deposition are mainly divided into direct
118 monitoring (such as dynamic chambers) and indirect monitoring (such as inferential
119 methods). The inferential model is widely applied in ground-based monitoring
120 networks (such as EANET and NNDMN), mainly because this method is more
121 practical and simpler. In inferential models, dry deposition is divided into two parts:
122 surface N_r concentrations and the deposition velocity (V_d) of N_r (Nowlan et al., 2014).
123 V_d can be estimated by meteorology, land use types of underlying surface as well as
124 the characteristics of each N_r component itself using resistance models (Nemitz et al.,
125 2001). Thus, dry N_r deposition monitoring networks only need to focus on the

126 quantification of surface concentration of individual N_r components. The N_r
127 components in the atmosphere are very complex, including N_2O_5 , HONO, NH_3 , NO_2 ,
128 HNO_3 and particulate NH_4^+ and NO_3^- . Most monitoring networks include the major
129 N_r species such as gaseous NH_3 , NO_2 , HNO_3 and the particles of NH_4^+ and NO_3^- .
130 Effort of ground-based N_r deposition monitoring mostly concentrates on wet N_r
131 deposition, while observations of dry N_r deposition are relatively scarce especially for
132 surface HNO_3 and NH_4^+ and NO_3^- . Second, most observation networks focus on a few
133 years or a certain period of time, leading to the lack of long-term continuously
134 monitoring on both wet and dry N_r deposition. More importantly, the global N_r
135 deposition monitoring network has not been established, and the sampling standards
136 in different regions are not unified. These outline the potential room for improvement
137 of ground-based N_r deposition monitoring.

138 **2.2 Atmospheric Chemistry Transport Model (ACTM) Simulation**

139 An ACTM can simulate N_r deposition at regional or global scales through explicitly
140 representing the physical and chemical processes of atmospheric N_r components
141 (Zhao et al., 2017; Zhang et al., 2012). Wet N_r deposition flux is parameterized as
142 in-cloud, under-cloud and precipitation scavenging (Amos et al., 2012; Levine and
143 Schwartz, 1982; Liu et al., 2001; Mari et al., 2000), while dry deposition flux can be
144 obtained as the product of surface N_r concentration and V_d , which is typically
145 parameterized as a network of resistances (Wesely and Hicks, 1977). Based on the
146 integrated results of 11 models of HTAP (hemispheric transport of air pollution), Tan
147 et al. found that about 76%-83% of the ACTM's simulation results were $\pm 50\%$ of the
148 monitoring values, and the modeling results underestimated the wet deposition of
149 NH_4^+ and NO_3^- over Europe and East Asia, and overestimated the wet deposition of
150 NO_3^- over the eastern US (Tan et al., 2018). Though regional ACTMs can be

151 configured at very high horizontal resolution (e.g., $1 \times 1 \text{ km}^2$) (Kuik et al., 2016), the
152 horizontal resolution of global ACTMs are relatively coarse ($1^\circ \times 1^\circ$ to $5^\circ \times 4^\circ$) (Williams
153 et al., 2017), which cannot indicate the local pattern of N_r deposition. On the other
154 hand, the N_r emission inventory used to drive an ACTM is highly uncertain, with the
155 uncertainty of the NO_x emission at about $\pm 30\text{-}40\%$, and that of NH_3 emission at about
156 $\pm 30\text{-}80\%$ (Zhang et al., 2009; Cao et al., 2011).

157 **2.3 Satellite-based Estimation of Surface N_r Concentration and Deposition**

158 Satellite observation has wide spatial coverages and high resolution, and is
159 spatiotemporally continuous. Atmospheric NO_2 and NH_3 columns can be derived
160 from satellite measurements with relatively high accuracy (Van Damme et al.,
161 2014a; Boersma et al., 2011), providing a new perspective about atmospheric N_r
162 abundance.

163 Satellite instruments that can monitor NO_2 in the atmosphere include GOME (Global
164 Ozone Monitoring Experience), SCIAMACHY (SCanning Imaging Absorption
165 SpectroMeter for Atmospheric ChartographY), OMI (Ozone Monitoring Instrument),
166 GOME-2 (Global Ozone Monitoring Experience-2). Some scholars applied satellite
167 NO_2 columns to estimate the surface NO_2 concentration, and then dry NO_2 deposition
168 by combining the surface NO_2 concentration and modeled V_d . Cheng et al. established
169 a statistical model to estimate the surface NO_2 concentration based on the
170 SCIAMACHY NO_2 columns, and then estimated the dry deposition of NO_2 over
171 eastern China (Cheng et al., 2013). This method used the simple linear model and did
172 not consider the vertical profiles of NO_2 (Cheng et al., 2013). Lu et al. established a
173 multivariate linear regression model based on the SCIAMACHY and GOME NO_2
174 columns, meteorological data and ground-based monitoring N_r deposition, and then
175 estimated the global total N_r deposition (Lu et al., 2013). Lu et al. could not

176 distinguish the contribution of dry and wet N_r deposition using the multivariate linear
177 regression model (Lu et al., 2013). Jia et al. established a simple linear regression
178 model based on OMI tropospheric NO_2 column and ground-based surface N_r
179 concentration, and then estimated the total amounts of dry N_r deposition (Jia et al.,
180 2016). Jia et al. used OMI tropospheric NO_2 column to estimate the dry deposition of
181 reduced N_r deposition (NH_3 and NH_4^+), which could also bring great errors since the
182 OMI NO_2 column could not indicate the NH_3 emission. These studies highlight the
183 problem of using only NO_2 columns to derive total N_r deposition, that NO_2 columns
184 give us highly limited information about the abundance of reduced N_r (NH_3 and
185 NH_4^+).

186 Lamsal et al. first used the relationship between the NO_2 column and surface NO_2
187 concentration at the bottom layer simulated by an ACTM to convert OMI NO_2
188 column to surface NO_2 concentration (Lamsal et al., 2008). A series of works (Lamsal
189 et al., 2013; Nowlan et al., 2014; Kharol et al., 2018) have effectively estimated
190 regional and global surface NO_2 concentration using satellite NO_2 column combining
191 with ACTM-derived relationship between the NO_2 column and surface NO_2
192 concentration simulated. It is worth mentioning that Nowlan et al. applied OMI NO_2
193 column to obtain the global dry NO_2 deposition during 2005-2007 for the first time
194 (Nowlan et al., 2014). However, using satellite NO_2 column and ACTM-derived
195 relationship between the NO_2 column and surface NO_2 concentration may lead to an
196 underestimation of surface NO_2 concentration. Kharol et al. found that the
197 satellite-derived surface NO_2 concentration using the above method is only half of the
198 observed values (Kharol et al., 2015). To resolve such potential underestimation,
199 Larkin et al. established a statistical relationship between the satellite-derived and
200 ground measured surface NO_2 concentration, and then calibrated the satellite-derived

201 surface NO₂ concentration using the established relationship (Larkin et al., 2017).
202 Some researchers also estimated other N_r components (such as particulate NO₃⁻)
203 based on satellite NO₂ column. Based on the linear model between NO₂, NO₃⁻, HNO₃
204 obtained by ground-based measurements, Jia et al. calculated the surface NO₃⁻ and
205 HNO₃ concentration using satellite-derived surface NO₂ concentration and their
206 relationship (Jia et al., 2016). Geddes et al. reconstructed the NO_x emission data by
207 using the satellite NO₂ column, and then estimated the global NO_x deposition by an
208 ACTM, but the spatial resolution of global NO_x deposition remains low (2 °×2.5 °),
209 failing to exploit the higher resolution of satellite observation (Geddes and Martin,
210 2017).

211 Comparing with NO₂, the development of satellite NH₃ monitoring is relatively late.
212 Atmospheric NH₃ was first detected by the TES in Beijing and Los Angeles (Beer et
213 al., 2008). The IASI sensor also detected atmospheric NH₃ from a biomass burning
214 event in Greece (Coheur et al., 2009). Subsequently, many scholars began to develop
215 more reliable satellite NH₃ column retrievals (Whitburn et al., 2016; Van Damme et al.,
216 2014a), validate the satellite-retrieved NH₃ column with the ground-based observation
217 (Van Damme et al., 2014a; Dammers et al., 2016; Li et al., 2017), and compare the
218 satellite NH₃ column with the aircraft measured NH₃ column (Van Damme et al.,
219 2014b; Whitburn et al., 2016). In recent years, some scholars have carried out the
220 works of estimating surface NH₃ concentration based on satellite NH₃ column. Liu et
221 al. obtained the satellite-derived surface NH₃ concentration in China based on the
222 IASI NH₃ column coupled with an ACTM, and deepened the understanding of the
223 spatial pattern of surface NH₃ concentration in China (Liu et al., 2017b). Similarly,
224 Graaf et al. carried out the relevant work in Europe based on the IASI NH₃ column
225 coupled with an ACTM, and estimated the dry NH₃ deposition in West Europe (Van

226 der Graaf et al., 2018). Jia et al. first constructed the linear model between surface
227 NO_2 and NH_4^+ concentration based on ground monitoring data, and then calculated
228 the NH_4^+ concentration using satellite-derived surface NO_2 concentration and their
229 relationship (Jia et al., 2016). However, as the emission sources of NO_x (mainly from
230 transportation and energy sectors) and NH_3 (mainly from agricultural sector) are
231 different (Hoesly et al., 2018), the linear model between surface NO_2 and NH_4^+
232 concentration may lead to large uncertainties in estimating the global NH_4^+
233 concentration. There is still no report about the satellite-derived dry and wet reduced
234 N_r deposition using satellite NH_3 column at a global scale. As reduced N_r plays an
235 important role in total N_r deposition, satellite NH_3 should be better utilized to help
236 estimate reduced N_r deposition.

237 **2.4 Problems in Estimating Global N_r Deposition**

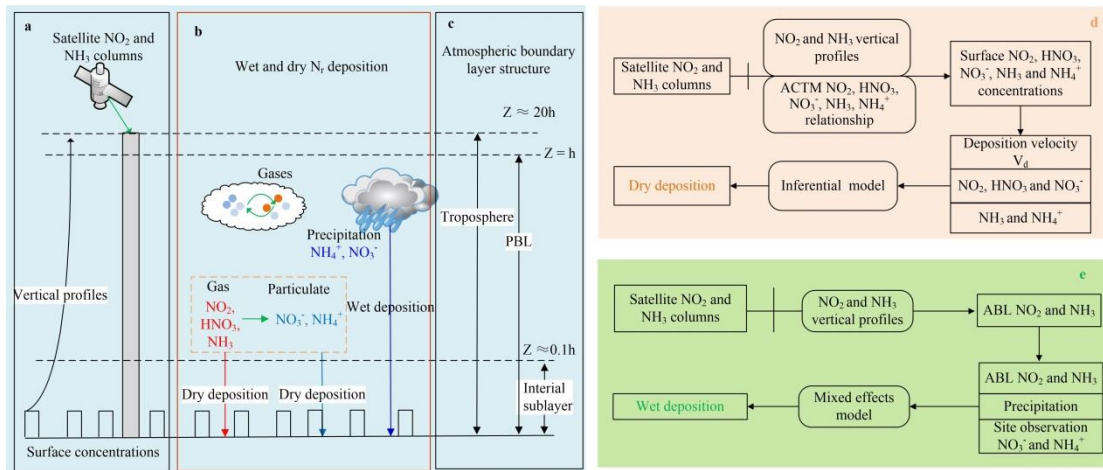
238 The spatial coverage of ground monitoring sites focusing on N_r deposition is still not
239 adequate, and the monitoring standards and specifications in different regions of the
240 world are not consistent, presenting a barrier to integrating different regional
241 monitoring data. Large uncertainties exist in N_r emission inventory used to drive the
242 ACTMs, and the spatial resolution of the modeled N_r deposition by ACTMs is coarse.
243 Using satellite monitoring data to estimate surface N_r concentration and deposition is
244 still in its infancy, especially for reduced N_r .

245 Some scholars tried to use satellite NO_2 and NH_3 column to estimate the surface N_r
246 concentration and dry N_r deposition. However, there are relatively few studies on
247 estimating wet N_r deposition. In addition, the development of satellite monitoring for
248 NH_3 in the atmosphere is relatively late (compared with NO_2). At present, IASI NH_3
249 data have been widely used, while the effective measurements of TES are less than
250 IASI; CrIS and AIRS NH_3 column products are still under development. There are

251 three main concerns in high-resolution estimation of surface N_r concentration and
 252 deposition based on satellite N_r observation. (1) How to effectively couple the satellite
 253 high-resolution NO_2 and NH_3 column data with the vertical profiles simulated by an
 254 ACTM, and then estimates the surface N_r concentrations? This step is the key to
 255 simulate the dry N_r deposition. (2) How to construct a model for estimating dry N_r
 256 deposition including all major N_r species based on satellite NO_2 and NH_3 column, and
 257 then estimates the dry N_r deposition at a high spatial resolution? (3) How to combine
 258 the high-resolution satellite NO_2 and NH_3 column data and ground-based monitoring
 259 data to construct wet N_r deposition models, and then estimate the wet N_r deposition at
 260 a high spatial resolution?

261 3. Framework of Estimating Surface N_r Concentration and Deposition Using 262 Satellite Observation

263 We give a framework of using satellite observation to estimate surface N_r
 264 concentration and deposition as shown in **Fig. 1** based on recent advances.



265
 266 **Fig. 1 Schematic diagram of dry and wet N_r deposition.** (a) indicates satellite observed NO_2
 267 and NH_3 column, and the vertical profiles by an ACTM; (b) shows dry and wet N_r deposition
 268 including the major N_r species (gaseous NO_2 , HNO_3 , NH_3 , particulate NO_3^- and NH_4^+ , as well as
 269 wet NO_3^- and NH_4^+ in precipitation); (c) illustrates atmospheric vertical structures including the
 270 troposphere (satellite observation), atmospheric boundary layer (ABL), interfacial sub-layer;
 271 (d) and (e) represent procedures of calculating the dry and wet N_r deposition.
 272

273 **3.1 Conversion of Satellite NO₂ and NH₃ Column to Surface N_r Concentration**

274 An ACTM can simulate the vertical profiles of NO₂ and NH₃ with multiple layers
275 from the surface to the troposphere. For example, the GEOS-Chem ACTM includes
276 47 vertical layers from the earth surface to the top of the stratosphere. Most previous
277 studies estimated the ratio of surface N_r concentration (at the first layer) to total
278 columns by an ACTM, and then multiply the ratio by satellite columns to estimate
279 satellite-derived surface concentration (Geddes et al., 2016;Graaf et al., 2018;Nowlan
280 et al., 2014).

281 Another approach tries to fit general vertical profiles of NO₂ and NH₃ (Zhang et al.,
282 2017;Liu et al., 2017b;Liu et al., 2017c), and then estimate the ratio of N_r
283 concentration at any height to total N_r columns, and finally multiply the ratio by
284 satellite NO₂ and NH₃ columns. This approach has an advantage compared with the
285 previous one for that NO₂ and NH₃ concentration at all altitude included in ACTM
286 simulations can be estimated.

287 Taking the estimation of surface NO₂ concentration using the latter approach as an
288 example, the methods and steps are introduced in the following.

289 Step 1: Calculate the monthly mean NO₂ concentrations at all layers simulated by an
290 ACTM.

291 Step 2: Construct the vertical profile function of NO₂. Multiple Gaussian functions are
292 used to fit the vertical distribution of NO₂ based on the monthly NO₂ concentrations at
293 all layers calculated in Step 1, in which the independent variable is the height
294 (altitude), and the dependent variable is NO₂ concentration at a certain height.

295 The basic form of single Gaussian function is (Zhang et al., 2017;Liu et al., 2017b;Liu
296 et al., 2017c;Whitburn et al., 2016):

$$297 \rho = \rho_{\max} e^{-\left(\frac{z-z_0}{\sigma}\right)^2} \quad (1)$$

298 where Z is the height of a layer in the ACTM; ρ_{\max} , Z_0 and σ are the maximum NO_2
 299 concentration, the corresponding height with the maximum NO_2 concentration and the
 300 thickness of NO_2 concentration layer (one standard error of Gaussian function).

301 There are two basic forms of profile shapes of NO_2 : (1) NO_2 concentration reaches the
 302 maximum concentration when reaching a certain height ($Z_0 \neq 0$). As the height
 303 increases, the NO_2 concentration begins to decline; (2) NO_2 concentration is basically
 304 concentrated on the earth surface ($Z_0 = 0$). These two cases are the ideal state of the
 305 vertical distribution of NO_2 concentration. In reality, single Gaussian fitting may not
 306 capture the vertical distribution of NO_2 well. To improve the accuracy of fitting, the
 307 sum of multiple Gaussian functions can be used (Liu et al., 2019):

$$308 \quad \rho(Z) = \sum_{i=1}^n \rho_{\max,i} e^{-\left(\frac{Z-Z_{0,i}}{\sigma_i}\right)^2} \quad (2)$$

309 Step 3: Calculate the ratio of NO_2 concentration at the height of h_G to total columns
 310 ($\int_0^{h_{\text{trop}}} \rho(Z) dx$), and then multiply the ratio by satellite column (S_{trop}). The
 311 satellite-derived N_r concentration at the height of h_G can be calculated as:

$$312 \quad S_{G_NO_2} = S_{\text{trop}} \times \frac{\rho(h_G)}{\int_0^{h_{\text{trop}}} \rho(Z) dx} \quad (3)$$

313 Step 4: Convert the instantaneous satellite-derived surface NO_2 concentration ($S_{G_NO_2}$)
 314 to daily average ($S_{G_NO_2}^*$) using the ratio of average surface NO_2 concentration
 315 (G_{ACTM}^{1-24}) to that at satellite overpass time ($G_{\text{ACTM}}^{\text{overpass}}$) by an ACTM (Liu et al., 2020):

$$316 \quad S_{G_NO_2}^* = \frac{G_{\text{ACTM}}^{1-24}}{G_{\text{ACTM}}^{\text{overpass}}} \times S_{G_NO_2} \quad (4)$$

317 The method for estimating the surface NH_3 concentration ($S_{G_NH_3}^*$) is similar to that
 318 for estimating the surface NO_2 concentration.

319 **3.2 Estimating Surface Concentration of Other N_r Species**

320 At present, only NO_2 and NH_3 column can be retrieved reliably, and there are no

321 reliable satellite retrievals of HNO₃, NH₄⁺ and NO₃⁻. For example, the IASI HNO₃
 322 product is still in the stage of data development and verification (Ronsmans et al.,
 323 2016). Previous studies firstly derive the relationship between N_r species by an
 324 ACTM or by ground-based measurements, and then use the relationship to convert
 325 satellite-derived surface NO₂ and NH₃ concentration (S_{G_NH3} *) to HNO₃, NH₄⁺ and
 326 NO₃⁻ concentrations:

$$327 \begin{cases} G_{S_NO3} = S_{G_NO2} * \times \frac{G_{ACTM_NO3}}{G_{ACTM_NO2}} \\ G_{S_HNO3} = S_{G_NO2} * \times \frac{G_{ACTM_HNO3}}{G_{ACTM_NO2}} \\ G_{S_NH4} = S_{G_NH3} * \times \frac{G_{ACTM_NH4}}{G_{ACTM_NH3}} \end{cases} (5)$$

328 $\frac{G_{ACTM_NO3}}{G_{ACTM_NO2}}$, $\frac{G_{ACTM_HNO3}}{G_{ACTM_NO2}}$, $\frac{G_{ACTM_NH4}}{G_{ACTM_NH3}}$ is the estimated ratio of between NO₂ and NO₃⁻,
 329 NO₂ and HNO₃, NH₃ and NH₄⁺.

330 3.3 Dry Deposition of N_r

331 The resistance of dry N_r deposition mainly comes from three aspects: aerodynamic
 332 resistance (R_a), quasi laminar sub-layer resistance (R_b) and canopy resistance (R_c).

333 The V_d can be expressed as

$$334 V_d = \frac{1}{R_a + R_b + R_c} + v_g \quad (6)$$

335 V_g is gravitational settling velocity. For gases, the V_g is negligible (V_g=0).

336 Dry NO₂, NO₃⁻, HNO₃, and NH₄⁺ deposition can be calculated by:

$$337 F = G_S \times V_d \quad (7)$$

338 Unlike above species, NH₃ is bi-directional, presenting both upward and downward
 339 fluxes. There is a so-called “canopy compensation point” (C_o) controlling dry NH₃
 340 deposition. Dry NH₃ deposition can be calculated by:

$$341 F = (G_{S_NH3} - C_o) \times V_d \quad (8)$$

342 The calculation of C_o is very complex including the leaf stomatal and soil emission

343 potentials related to the meteorological factors, the plant growth stage and the canopy
 344 type. The satellite-based methods usually neglected this complex process and set C_o
 345 as zero (Graaf et al., 2018;Kharol et al., 2018) or set fixed values in each land use
 346 type based on ground-based measurements (Jia et al., 2016).

347 **3.4 Wet Deposition of N_r**

348 The satellite-based estimation of wet N_r deposition can be simplified as the product of
 349 the concentration of N_r (C), precipitation (P) and scavenging coefficient (w) (Pan et
 350 al., 2012). Satellite NO_2 and NH_3 can be used to indicate the oxidized N_r and reduced
 351 N_r ; precipitation (P) can be obtained from ground monitoring data or reanalysis data
 352 (such as NCEP). However, the scavenging coefficient (w) is usually highly uncertain.
 353 To improve the accuracy of estimation, a mixed-effects model (Liu et al.,
 354 2017a;Zhang et al., 2018) is proposed to build the relationship between satellite NO_2
 355 and NH_3 , precipitation and ground monitoring wet N_r deposition:

$$356 \text{Wet}N_{ij} = \alpha_j + \beta_i \times P_{ij} \times (S_{ABL})_{ij} + \varepsilon_{ij} \quad (9)$$

$$357 S_{ABL} = S_{trop} \times \frac{\int_0^{ABL} \rho(Z)dx}{\int_0^{h_{trop}} \rho(Z)dx} \quad (10)$$

358 $\text{Wet}N_{ij}$ is wet NO_3^-N or NH_4^+N deposition at month i and site j ; $(S_{ABL})_{ij}$ is the
 359 atmospheric boundary layer (ABL) NO_2 or NH_3 columns at month i and site j ; P_{ij} is
 360 precipitation at month i and site j ; β_i and α_j are the slope and intercept of random
 361 effects, representing seasonal variability and spatial effects; ε_{ij} represents the random
 362 error at month i and site j .

363 The scavenging process of wet N_r deposition usually starts from the height of rainfall
 364 rather than the top of the troposphere, so it is more reasonable to use NO_2 and NH_3
 365 column below the height of rainfall to build the wet N_r deposition model. The NO_2
 366 and NH_3 column within ABL is used to build the wet deposition model since

367 precipitation height is close to the height of the ABL (generally less than 2-3 km).

368 **4. Satellite-derived Surface N_r Concentration and Deposition**

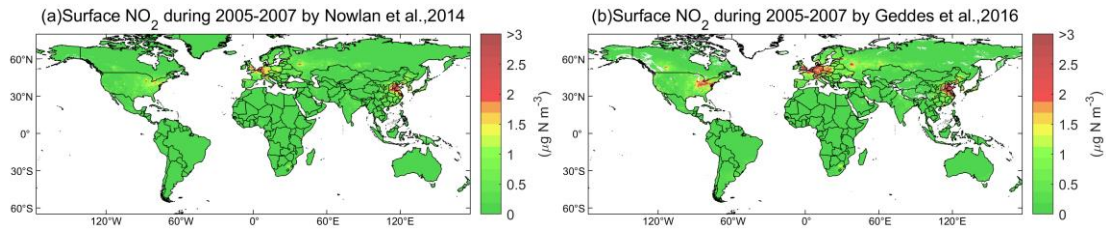
369 **4.1 Surface NO_2 Concentration and Oxidized N_r Deposition**

370 The spatial resolutions of global ACTMs and therefore modeled surface N_r
371 concentration are very coarse (for example, the spatial resolution of the global version
372 of GEOS-Chem is $2^\circ \times 2.5^\circ$). Thus it can be hard to estimate surface N_r concentration
373 and deposition at a fine resolution at a global scale by ACTMs alone. Instead, the
374 satellite N_r retrievals have a high spatial resolution and can reveal more spatial details
375 than ACTM simulations.

376 Cheng et al. and Jia et al. established a linear model between the surface NO_2
377 concentration and NO_2 column by assuming the ratio of the surface NO_2
378 concentration to the tropospheric NO_2 column to be fixed, and then used the linear
379 model to convert satellite NO_2 columns to surface NO_2 concentration, and finally
380 estimated dry NO_2 deposition using the inferential method (Cheng et al., 2013; Jia et
381 al., 2016). However, these statistical methods are highly dependent on the
382 ground-based measurements, and the established linear models may be not effective
383 over regions with few monitoring sites.

384 A comprehensive study (Nowlan et al., 2014) estimated global surface NO_2
385 concentration during 2005-2007 by multiplying OMI tropospheric NO_2 columns by
386 the ACTM-modeled ratio between surface NO_2 concentration and tropospheric
387 column (**Fig. 2**). Nowlan et al. also estimated dry NO_2 deposition using the
388 OMI-derived surface NO_2 concentration combining the modeled V_d during 2005-2007
389 (Nowlan et al., 2014). This approach followed an earlier study (Lamsal et al., 2008),
390 that focus on North America. As reported by Lamsal et al., the satellite-derived
391 surface NO_2 concentration was generally lower than ground-based NO_2 observations,

392 ranging from -17% to -36% in North America (Lamsal et al., 2008). Kharol et al. used
 393 a similar method and found the satellite-derived surface NO₂ concentration was only
 394 half of the ground-measured values in North America (Kharol et al., 2015).

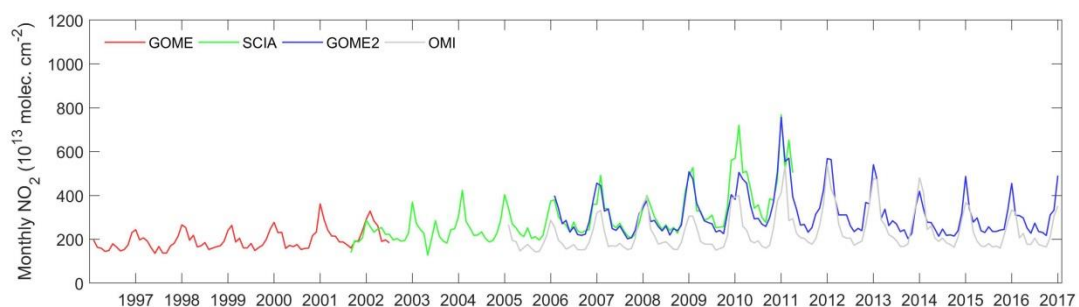


395

396 **Fig. 2** Satellite-derived surface NO₂ concentration during 2005-2007 by Nowlan et al. (Nowlan et
 397 al., 2014) (a) and by Geddes et al. (Geddes et al., 2016) (b). We gained the surface NO₂
 398 concentration by Nowlan et al. (Nowlan et al., 2014) and by Geddes et al. (Geddes et al., 2016) at
 399 the web: http://fizz.phys.dal.ca/~atmos/martin/?page_id=232.

400

401 Geddes et al. followed previous studies, and used NO₂ column from the GOME,
 402 SCIAMACHY, and GOME-2 to estimate surface NO₂ concentration (Geddes et al.,
 403 2016). Although Geddes et al. did not evaluate their results with ground-based
 404 observation (Geddes et al., 2016), it is obvious that their surface NO₂ estimates were
 405 higher than Nowlan's estimates based on OMI (Nowlan et al., 2014) (**Fig. 2**). This
 406 may be because the OMI-derived NO₂ column is much lower than that derived by
 407 GOME, SCIAMACHY, and GOME-2, especially over polluted regions. For example,
 408 in China, the OMI NO₂ column is about 30% lower than that of SCIAMACHY and
 409 GOME-2 consistently (**Fig. 3**).



410

411 **Fig. 3** An example of the time series of monthly NO₂ column retrieved by GOME, SCIAMACHY,
 412 GOME2 and OMI in China. We obtained the GOME, SCIAMACHY, GOME2 and OMI data from
 413 <http://www.temis.nl/airpollution/no2.html>.

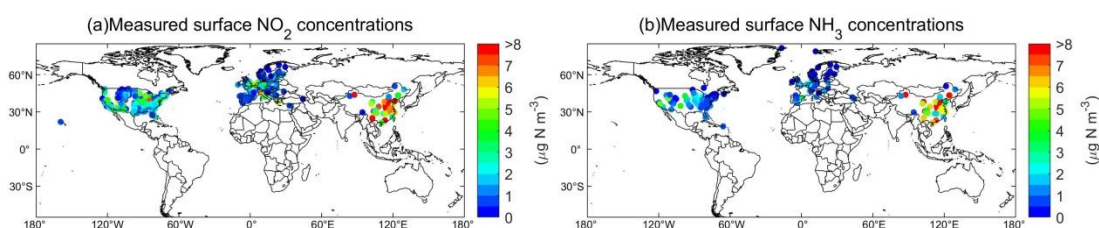
414

415 Larkin et al. established a land-use regression model to estimate global surface NO₂

416 concentration by combining satellite-derived surface NO₂ concentration by Geddes et
417 al. and ground-based annual NO₂ measurements (Geddes et al., 2016;Larkin et al.,
418 2017). The study by Larkin et al. can be considered as using the ground-based annual
419 measurements to adjust the satellite-derived surface NO₂ concentration by Geddes et
420 al. (Geddes et al., 2016;Larkin et al., 2017), which helped reduce the discrepancy
421 between satellite-derived and ground-measured NO₂ concentration. The regression
422 model captured 54% of global NO₂ variation, with an absolute error of 2.32 μg N m⁻³.
423 Zhang et al. followed the framework in **Sect. 3** to estimate the OMI-derived surface
424 NO₂ concentration (at ~50 m) in China, and found good agreement with ground-based
425 surface NO₂ concentration from the NNDMN at yearly scale (slope=1.00, R²=0.89)
426 (Zhang et al., 2017). The methods by Zhang et al. can also generate OMI-derived NO₂
427 concentration at any height by the constructed NO₂ vertical profile (Zhang et al.,
428 2017). Zhang et al. also estimated dry NO₂ deposition using the OMI-derived surface
429 NO₂ concentration combining the modeled V_d during 2005-2016 (Zhang et al., 2017).
430 Based on Zhang's estimates, the Gaussian function can well simulate the vertical
431 distribution of NO₂ from an ACTM (MOZART) (Emmons et al., 2010) with 99.64%
432 of the grids having R² values higher than 0.99. This suggests that the
433 ACTM-simulated vertical distribution of NO₂ has a general pattern, which can be
434 emulated by Gaussian functions. Once a vertical profile was constructed, it can be
435 easily used to estimate NO₂ concentration at any height.

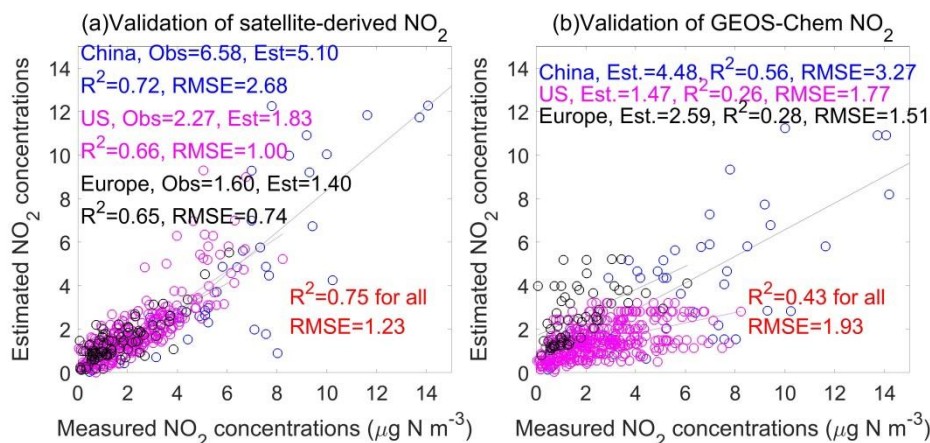
436 In this study, we used the framework in **Sect. 3** to estimate the OMI-derived surface
437 NO₂ concentration globally. To validate the OMI-derived surface NO₂ concentrations,
438 ground-measured surface NO₂ concentration in China, the US and Europe in 2014
439 was collected (**Fig. 4**). The total number of NO₂ observations in China, the US and
440 Europe are 43, 373 and 88 respectively. The OMI-derived annual average for all sites

441 was $3.74 \mu\text{g N m}^{-3}$, which was close to the measured average ($3.06 \mu\text{g N m}^{-3}$). The R^2
 442 between OMI-derived surface NO_2 concentrations and ground-based NO_2
 443 measurements was 0.75 and the RMSE was $1.23 \mu\text{g N m}^{-3}$ (**Fig. 5**), which is better
 444 than the modeling results by the GEOS-Chem ACTM ($R^2=0.43$, $\text{RMSE}=1.93 \mu\text{g N}$
 445 m^{-3}). Satellite-based methods have the advantages of spatiotemporally continuous
 446 monitoring N_r at a higher resolution, which helps alleviate the problem of the coarse
 447 resolution of ACTMs in estimating N_r concentration and deposition.



448

449 **Fig. 4** Spatial distribution of measured surface NO_2 and NH_3 concentrations in 2014. For NO_2 (a),
 450 the measured data in China, the US and Europe were obtained from the NNDMN, US-EPA and
 451 EMEP, respectively; for NH_3 (b), the measured data in China, the US and Europe were obtained
 452 from the NNDMN, US-AMoN and EMEP, respectively
 453

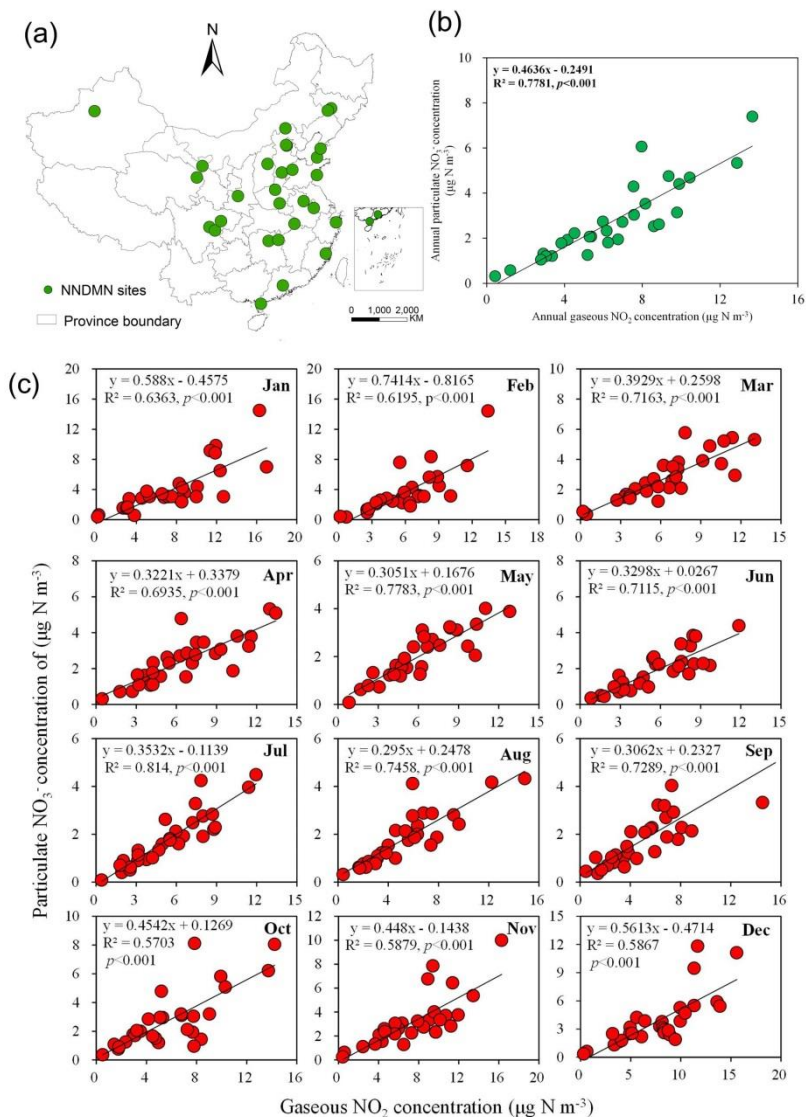


454

455 **Fig. 5** Comparison between annual mean satellite-derived and ground-measured surface NO_2
 456 concentrations (a), and comparison between annual mean modeled (by an ACTM as GEOS-Chem)
 457 and ground-measured surface NO_2 concentrations (b). The ground-based monitoring sites are
 458 shown in **Fig. 4**.
 459

460 For NO_3^- and HNO_3 , previous studies firstly constructed the relationship between NO_2 ,
 461 NO_3^- and HNO_3 , and found a relatively high linear relationship between NO_2 , NO_3^- ,
 462 and HNO_3 at a monthly or yearly scale. For example, Jia et al. found a linear

463 relationship between NO_2 and NO_3^- , HNO_3 concentration at annual scale ($R^2=0.70$)
464 (Jia et al., 2016). Similarly, based on the ground-based measurements in the NNDMN,
465 a high correlation was found between surface NO_2 and NO_3^- concentration at monthly
466 or annual timescales (**Fig. 6**) (Liu et al., 2017c). Using these linear relationships and
467 satellite-derived surface NO_2 concentration, the annual mean surface NO_3^- and HNO_3
468 can be estimated. Alternatively, the relationship of NO_2 , NO_3^- and HNO_3 can also be
469 modeled by an ACTM. For example, a strong relationship of tropospheric NO_2 , NO_3^-
470 and HNO_3 column was simulated over all months by an ACTM, with the correlation
471 ranging from 0.69 to 0.91 (Liu et al., 2017a). But, over shorter timescales, the
472 relationship between NO_2 , NO_3^- and HNO_3 may be nonlinear, which we should be
473 cautious about when estimating surface NO_3^- and HNO_3 concentration from NO_2
474 concentration.



475

476 **Fig. 6** Correlation between surface NO_2 and particulate NO_3^- concentration in the NNDMN at
 477 annual and monthly scales, which were adopted from our previous study (Liu et al., 2017c). (a)
 478 indicates the spatial locations of monitoring sites in the NNDMN; (b) and (c) represent yearly and
 479 monthly relationship between surface NO_2 and particulate NO_3^- concentration, respectively.

480

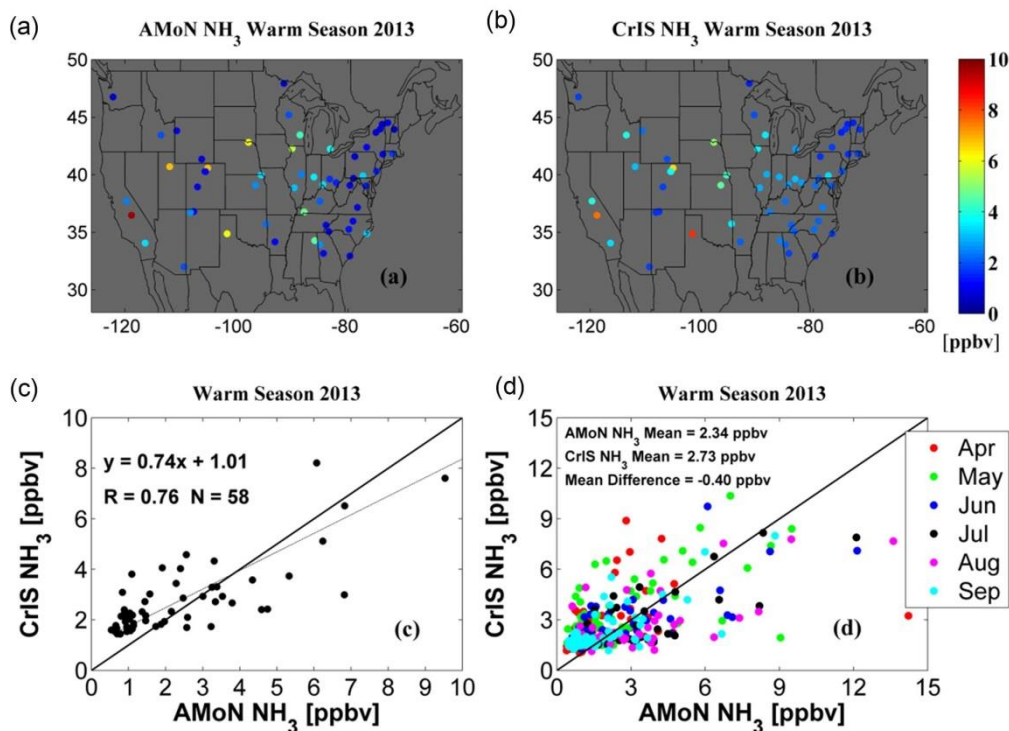
481 For the wet N_r deposition, Liu et al. followed the framework in **Sect. 3** to estimate wet
 482 nitrate deposition using ABL NO_2 columns derived from OMI NO_2 column and NO_2
 483 vertical profile from an ACTM (MOZART), and precipitation by a mixed-effects
 484 model showing the proposed model can achieve high predictive power for monthly
 485 wet nitrate deposition over China ($R=0.83$, $\text{RMSE}=0.72$) (Liu et al., 2017a).

486 4.2 Surface NH_3 Concentration and Reduced N_r Deposition

487 With the development of atmospheric remote sensing of NH_3 , some scholars have

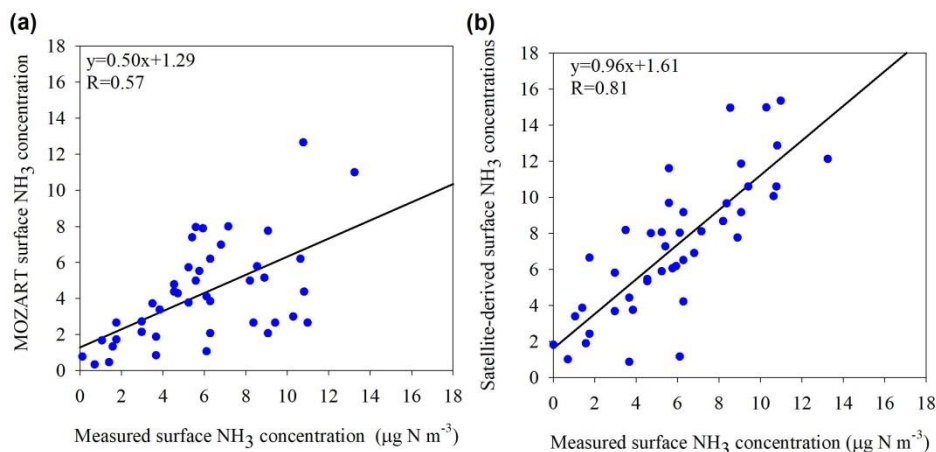
488 estimated surface NH_3 concentration and dry NH_3 deposition based on the satellite
489 NH_3 column data. Assuming the ratio between the surface NH_3 concentration to the
490 NH_3 column was fixed, Yu et al. applied a linear model to convert satellite NH_3
491 columns to surface NH_3 concentration and estimated dry NH_3 deposition in China
492 using the inferential method (Yu et al., 2019). But Yu et al. did not consider the spatial
493 variability of the vertical profiles of NH_3 (Yu et al., 2019), which may cause a large
494 uncertainty in estimating surface NH_3 concentration.

495 In Western Europe, Graaf et al. used the ratio of the surface NH_3 concentration (in the
496 bottom layer) to total NH_3 column from an ACTM to convert the IASI NH_3 column to
497 surface NH_3 concentration, and then estimated dry NH_3 deposition combining the
498 modeled deposition velocity and IASI-derived surface NH_3 concentration (Graaf et al.,
499 2018). Similarly, in North America, Kharol et al. estimated the dry NH_3 deposition by
500 the CrIS-derived surface NH_3 concentration and deposition velocity of NH_3 (Kharol et
501 al., 2018). They found a relatively high correlation ($R=0.76$) between the
502 CrIS-derived surface NH_3 concentration and AMoN measurements during warm
503 seasons (from April to September) in 2013 (**Fig. 7**). Over China, Liu et al. found a
504 higher correlation ($R=0.81$) between IASI-derived surface NH_3 concentrations and the
505 measured surface NH_3 concentrations than those from an ACTM ($R=0.57$, **Fig. 8**)
506 (Liu et al., 2017b).



507

508 **Fig. 7** Comparisons of the measured surface NH₃ concentration by the AMoN and CrIS-derived
 509 surface NH₃ concentration in the US during warm season (April-September) in 2013 (Kharol et al.,
 510 2018). (a) and (b) indicate measured and CrIS-derived surface NH₃ concentration at the AMoN
 511 sites, respectively; (c) represents the comparison of averaged surface NH₃ concentration during
 512 warm months between CrIS-derived estimates and measurements, while (d) indicates the
 513 comparison of monthly surface NH₃ concentration between CrIS-derived estimates and
 514 measurements.
 515

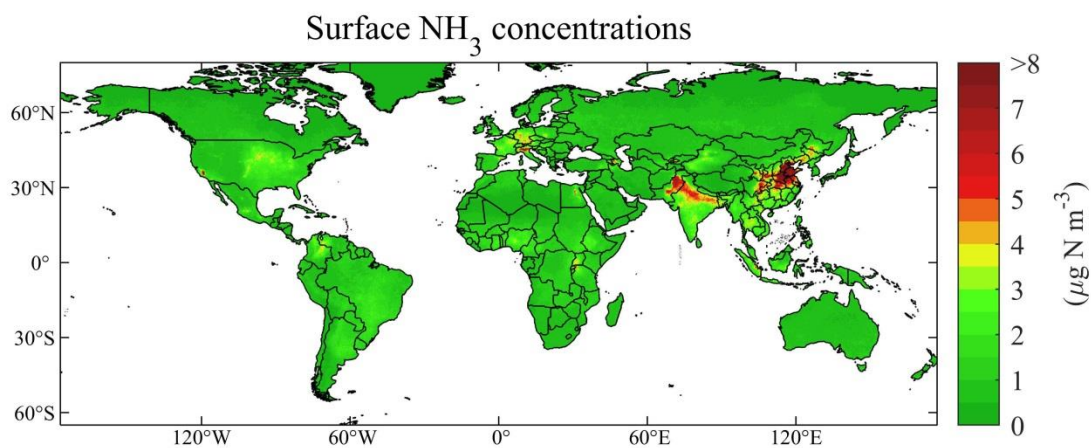


516

517 **Fig. 8** Comparisons of the measured surface NH₃ concentration with IASI-derived surface NH₃
 518 concentration at the NNDMN sites over China (Liu et al., 2017b). (a) indicates the comparison of
 519 measured and modeled surface NH₃ concentration from an ACTM (MOZART), and (b) represents
 520 the comparison of the measured and IASI-derived surface NH₃ concentration.
 521

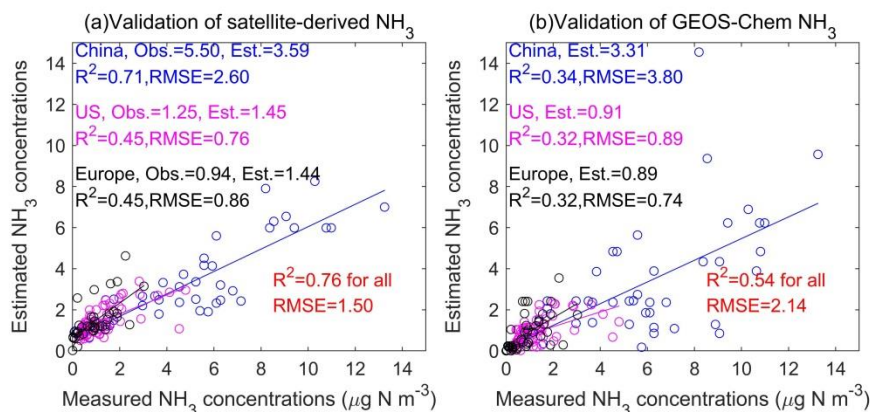
522 Liu et al. followed the framework in **Sect. 3** to estimate the IASI-derived surface NH₃
 523 concentration (at the middle height of the first layer by an ACTM) (**Fig. 9**), and found

524 a good agreement with ground-based surface NH₃ concentration (Liu et al., 2019).
525 The correlation between the measured and satellite-derived annual mean surface NH₃
526 concentrations over all sites was 0.87 as shown in **Fig. 10**, while the average
527 satellite-derived and ground-measured surface NH₃ concentration was 2.52 and 2.51
528 $\mu\text{g N m}^{-3}$ in 2014 at the monitoring sites, respectively. The satellite-derived estimates
529 achieved a better accuracy ($R^2=0.76$, RMSE = $1.50 \mu\text{g N m}^{-3}$) than an ACTM
530 (GEOS-Chem, $R^2=0.54$, RMSE = $2.14 \mu\text{g N m}^{-3}$). The satellite NH₃ retrievals were
531 affected by the detection limits of the satellite instruments and thermal contrast.
532 Higher correlation over China than other regions for the satellite estimates was linked
533 to the detection limits by the instruments and thermal contrast (Liu et al., 2019).
534 Higher accuracy could be gained with higher thermal contrast and NH₃ abundance.
535 Instead, the uncertainties of NH₃ retrievals would be higher with lower thermal
536 contrast and NH₃ abundance.



537

538 **Fig. 9** Spatially satellite-based surface NH₃ estimates in 2014 (Liu et al., 2019). The global surface
539 NH₃ concentration datasets have been released on the website:
540 <https://zenodo.org/record/3546517#.Xj6I4GgzY2w>.
541

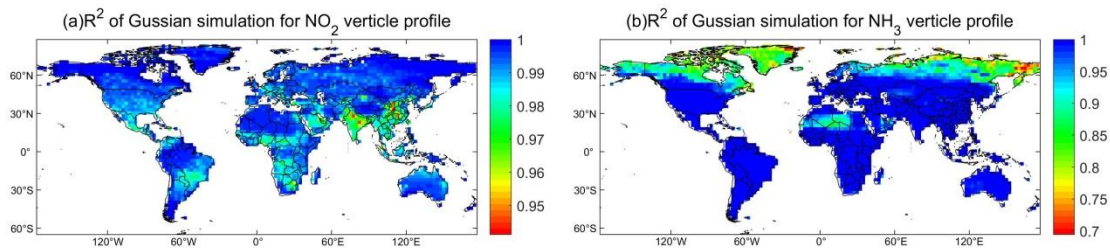


542

543 **Fig. 10** Comparison between yearly satellite-based and measured surface NH₃ concentrations (a),
 544 and comparison between yearly modeling (by an ACTM as GEOS-Chem) and measured surface
 545 NH₃ concentrations (b) (Liu et al., 2019). The ground-based monitoring sites are shown in **Fig. 4**.
 546

547 The proposed methods (Liu et al., 2019) can also estimate NH₃ concentration at any
 548 height using the constructed vertical profile function of NH₃. The Gaussian function
 549 can well emulate the vertical distribution of NH₃ from an ACTM outputs with 99% of
 550 the grids having R^2 values higher than 0.90 (**Fig. 11**). This means, for regional and
 551 global estimation, the vertical distribution of NH₃ concentration has a general pattern,
 552 which can be mostly emulated by the Gaussian function. Once a global NH₃ vertical
 553 profile was simulated, it can be easily used to estimate satellite-derived NH₃
 554 concentration at any height. We can also estimate dry NH₃ deposition using the
 555 IASI-derived surface NH₃ concentration combining the modeled V_d . For the dry
 556 deposition, the uncertainty mainly came from the satellite-derived estimates using the
 557 modeled vertical profiles. The uncertainty of vertical profiles modeled by the ACTM
 558 mainly resulted from the chemical and transport mechanisms. We recommend using
 559 the Gaussian function to determine the height of surface NO₂ and NH₃ concentrations
 560 that best matched with the ground-based measurements. There may exist systematic
 561 biases by simply using the relationship of NO₂ columns and surface concentration to
 562 estimate satellite surface NO₂ concentrations. To date, there are still no studies

563 developing satellite-based methods to estimate the wet reduced N_r deposition on a
564 regional scale.



565

566 **Fig. 11** Spatial distributions of R^2 for Gaussian function by simulating NH_3 and NO_2 vertical
567 profiles. This is an example of Gaussian fitting using 47 layers' NH_3 and NO_2 concentration from
568 an ACTM (GEOS-Chem).
569

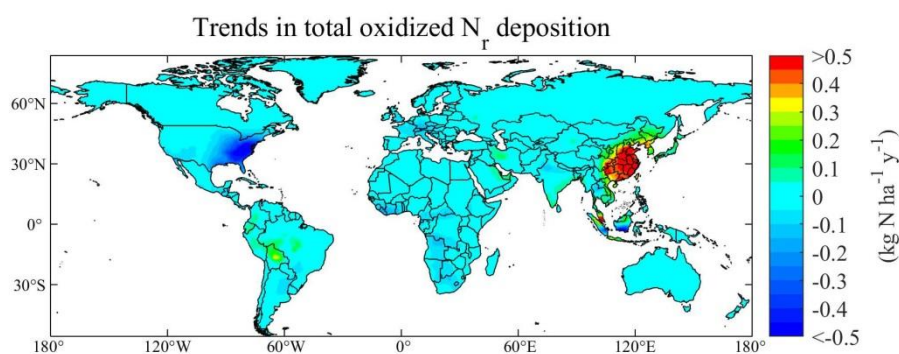
570 **5. Trends of Surface N_r Concentration and Deposition by Satellite-based**

571 **Methods**

572 The N_r concentration and deposition modeled by ACTMs are highly dependent on the
573 accuracy of input N_r emissions. The methods commonly used to estimate
574 anthropogenic N_r emissions are based on the data of human activities and emission
575 factors, which can be highly uncertain. The ACTM methods driven by N_r emission
576 inventory have relatively poor timeliness, and have limitations in monitoring the
577 recent trends of N_r deposition.

578 Satellite-based methods provide a simple, fast and relatively objective way to
579 monitoring N_r deposition at a high resolution, and less susceptible to the errors in the
580 assumptions that emission inventories are compiled based on, particularly the lack of
581 reliable data over developing countries (Crippa et al., 2018). With such advantages,
582 researchers developed the satellite-based methods to estimate surface N_r concentration,
583 deposition and even emissions. Satellite-based methods have advantages in
584 monitoring the recent trends of N_r deposition. Geddes et al. used NO_2 column from
585 the GOME, SCIAMACHY, and GOME-2 to estimate satellite-derived NO_x emissions,
586 and then used the calibrated NO_x emission inventory to drive an ACTM to simulate
587 the long-term oxidized N_r deposition globally (Geddes and Martin, 2017). They found

588 oxidized N_r deposition from 1996 to 2014 decreased by 60% in Eastern US, doubled
 589 in East China, and declined by 20% in Western Europe (**Fig. 12**). We use the datasets
 590 by Geddes et al. to calculate the trends of total oxidized N_r deposition during
 591 1996-2014 (Geddes and Martin, 2017). It is obvious that two completely opposite
 592 trends exist: (1) in East China with a steep increase of higher than $0.5 \text{ kg N ha}^{-1} \text{ y}^{-1}$
 593 and (2) East US with a steep decrease of lower than $-0.5 \text{ kg N ha}^{-1} \text{ y}^{-1}$. Although it is
 594 not a direct way to use satellite N_r observation to estimate N_r deposition, the method
 595 of estimating trends of N_r deposition by Geddes et al. can be considered effective
 596 since it took account of the changes of both NO_x emission and climate by an ACTM
 597 (Geddes and Martin, 2017).

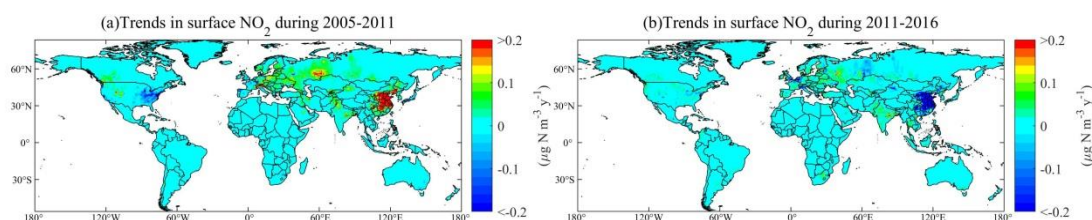


598

599 **Fig. 12** Gridded annual changes of total oxidized N_r deposition simulated by GEOS-Chem
 600 constrained with GOME, SCIAMACHY, and GOME-2 NO_2 retrievals during 1996-2014 (Geddes
 601 and Martin, 2017). We gained the generated datasets
 602 (http://fizz.phys.dal.ca/~atmos/martin/?page_id=1520) by Geddes et al., and calculated the trends
 603 using the linear methods.
 604

605 Some researchers developed a more direct way to infer the trends of surface N_r
 606 concentration and deposition. Geddes et al. presented a comprehensive long-term
 607 global surface NO_2 concentration estimate (at 0.1° resolution using an oversampling
 608 approach) between 1996 and 2012 by using NO_2 column from the GOME,
 609 SCIAMACHY, and GOME-2 (Geddes et al., 2016). The surface NO_2 concentration in
 610 North America (the US and Canada) decreased steeply, followed by Western Europe,
 611 Japan and South Korea, while approximately tripled in China and North Korea

612 (Geddes et al., 2016). Jia et al. established a simple linear regression model based on
 613 OMI NO₂ column and ground-based surface N_r concentration, and then estimated the
 614 trends of dry N_r deposition globally between 2005 and 2014 (Jia et al., 2016). They
 615 found that dry N_r deposition in Eastern China increased rapidly, while in the Eastern
 616 US, Western Europe, and Japan dry N_r deposition has decreased in recent decades.
 617 We split the time span of 2005-2016 into two periods: 2005-2011 and 2011-2016, as
 618 surface NO₂ concentration shows opposite trend in China in these two periods. The
 619 magnitudes of both growth and decline in surface NO₂ concentration in China are
 620 most pronounced worldwide in the two periods (**Fig. 13**). During 2005-2011, apart
 621 from Eastern China with the largest increase in surface NO₂ concentration, there are
 622 also several areas with increasing trends such as Northwest and East India (New Delhi
 623 and Orissa), Western Russia, Eastern Europe (Northern Italy), Western US (Colorado
 624 and Utah), Northwestern US (Seattle and Portland), Southwestern Canada (Vancouver,
 625 Edmonton, Calgary), Northeast Pakistan and Northwest Xinjiang (Urumqi). Notably,
 626 the biggest decreases in surface NO₂ concentration during 2005-2011 occurred in
 627 Eastern US and Western EU (North France, South England, and West German).
 628 During 2011-2016, due to the strict control of NO_x emissions, Eastern China had the
 629 largest decrease in surface NO₂ concentration than elsewhere worldwide, followed by
 630 Western Xinjiang, Western Europe and some areas in Western Russia.

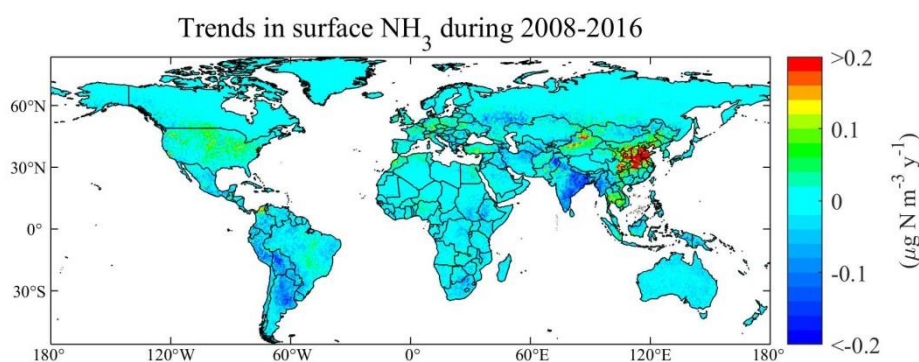


631

632 **Fig. 13** Gridded annual changes in surface NO₂ concentrations gained by OMI retrievals during
 633 2005-2011 (a) and during 2011-2016 (b) in this study. We have released the global surface NO₂
 634 concentrations during 2005-2016 available at the website:
 635 <https://zenodo.org/record/3546517#.Xj6I4GgzY2w>.
 636

637 Liu et al. estimated surface NH₃ concentration globally during 2008-2016 using

638 satellite NH₃ retrievals by IASI (Liu et al., 2019). A large increase of surface NH₃
639 concentrations was found in Eastern China, followed by Northern Xinjiang province
640 in China during 2008-2016 (**Fig. 14**). Satellite-based methods have been proven as an
641 effective and unique way to monitoring the trends of global N_r concentration and
642 deposition. To date, there are still few studies reporting the satellite-derived trends of
643 reduced N_r deposition on a global scale.



644

645 **Fig. 14** Gridded annual changes in surface NH₃ concentrations gained by IASI retrievals during
646 2008-2016 (Liu et al., 2019). We have released the global surface NH₃ concentrations during
647 2008-2016 at the website: <https://zenodo.org/record/3546517#.Xj6I4GgzY2w>.
648

649 **6. Remaining Challenges for Estimating N_r Deposition Using Satellite**

650 **Observation**

651 First, the reduced N_r deposition plays an important contribution to total N_r deposition.
652 NH₃ exhibits bi-directional air-surface exchanges. The NH₃ compensation point
653 (Farquhar et al., 1980) is also an important and highly variable factor controlling dry
654 NH₃ deposition (Schrader et al., 2016; Zhang et al., 2010). However, the current
655 existing satellite-based methods did not consider this bi-directional air-surface
656 exchange. It is important to better parameterize the NH₃ compensation point, and
657 assess the effects of bi-directional air-surface exchanges on estimating the dry NH₃
658 deposition.

659 Second, the existing satellite-based methods to estimate N_r deposition used the ratio
660 of the surface N_r concentration to the N_r column by an ACTM to convert satellite N_r

661 column to surface N_r concentration. However, the calculated ratio (by an ACTM) and
662 the satellite N_r column have different spatial resolutions, and previous studies usually
663 applied the modeled ratio directly or interpolate the ratio into the resolution of
664 satellite N_r column. This method assumes the relationship at coarse resolution by an
665 ACTM can also be effective in fine resolution as satellite indicated. When regional
666 studies are conducted, regional ACTMs coupled with another meteorological model
667 (e.g. WRF-Chem, WRF-CMAQ) (Grell et al., 2005; Wong et al., 2012) can be
668 configured to match the spatial resolution of satellite observation, but this is not as
669 viable for global ACTMs (e.g. MOZART, GEOS-Chem) due to differences in model
670 structures and computational cost. The modeled ratio of surface N_r concentration to
671 the N_r column may have variability at spatial scales finer than the horizontal
672 resolution of global ACTMs. The impact of such scale effect (at different spatial
673 scales) on estimated surface N_r concentration should be further studied.

674 Third, the satellite observation can only obtain reliable NO_2 and NH_3 column
675 presently, and there are no available high-resolution and reliable direct HNO_3 , NO_3^- ,
676 NH_4^+ retrievals. For HNO_3 , NO_3^- , NH_4^+ concentrations, the satellite-based methods
677 often applied the satellite-derived NO_2 and NH_3 concentration and the relationship
678 between N_r species from an ACTM (or ground-based measurements) to estimate
679 surface HNO_3 , NO_3^- , NH_4^+ concentration. With the development of satellite
680 technology, more and more N_r species can be detected, such as HNO_3 . However, at
681 present, satellite HNO_3 products are not mature, and the spatial resolution is low.
682 Direct, high-resolution and reliable satellite monitoring of more N_r species is critical
683 to further developing the use of using atmospheric remote sensing to estimate N_r
684 deposition at global and regional scales.

685 Fourth, estimating wet N_r deposition using satellite NO_2 and NH_3 column remains

686 relatively uncommon. Further studies should focus on how to combine the
687 high-resolution satellite NO_2 and NH_3 column and the ground-based monitoring data
688 to build wet N_r deposition models to estimate wet N_r deposition at higher
689 spatiotemporal resolution. The proposed scheme to estimate the wet N_r deposition in
690 **Sect. 3** is statistical. On the other hand, the wet N_r deposition includes the scavenging
691 processes of in-cloud, under-cloud and precipitation. Processed-level knowledge and
692 models can benefit the estimation of wet N_r deposition using satellite NO_2 and NH_3
693 column.

694 **7. Conclusion**

695 The recent advances of satellite-based methods for estimating surface N_r
696 concentration and deposition have been reviewed. Previous studies have focused on
697 using satellite NO_2 column to estimate surface NO_2 concentrations and dry NO_2
698 deposition both regionally and globally. The research on calculating surface NH_3
699 concentration and reduced N_r deposition by satellite NH_3 data is just beginning, and
700 some scholars have carried out estimating surface NH_3 concentration and dry NH_3
701 deposition on different spatial and temporal scales, but the research degree is still
702 relatively low. We present a framework of using satellite NO_2 and NH_3 column to
703 estimate N_r deposition based on recent advances. The proposed framework of using
704 Gaussian function to model vertical NO_2 and NH_3 profiles can be used to convert the
705 satellite NO_2 and NH_3 column to surface NO_2 and NH_3 concentration at any height
706 simply and quickly. The proposed framework of using satellite NO_2 and NH_3 column
707 to estimate wet N_r deposition is a statistical way, and further studies should be done
708 from a mechanism perspective. Finally, we summarized current challenges of using
709 satellite NO_2 and NH_3 column to estimate surface N_r concentration and deposition
710 including a lack of considering NH_3 bidirectional air-surface exchanges and the

711 problem of different spatial scales between an ACTM and satellite observation.

712 **Acknowledgments**

713 This study is supported by the National Natural Science Foundation of China (No.
714 41471343, 41425007 and 41101315) and the Chinese National Programs on Heavy
715 Air Pollution Mechanisms and Enhanced Prevention Measures (Project No. 8 in the
716 2nd Special Program).

717 **Author contributions.** LL designed this study. LL, YYY and WX conducted the data
718 analysis. All co-authors contributed to the revision of the paper.

719 **Data availability.** OMI NO₂ datasets are available at
720 <http://www.temis.nl/airpollution/no2.html>. IASI NH₃ datasets are available at
721 <https://cds-espri.ipsl.upmc.fr/etherTypo/index.php?id=1700&L=1>. Surface NO₂
722 concentration during 2005-2007 obtained by Nowlan et al. (Nowlan et al., 2014) and
723 longterm estimates (1996-2012) by Geddes et al. (Geddes et al., 2016) are available at
724 http://fizz.phys.dal.ca/~atmos/martin/?page_id=232. Total oxidized N_r deposition
725 simulated by GEOS-Chem constrained with GOME, SCIAMACHY, and GOME-2
726 NO₂ retrievals during 1996-2014 (Geddes and Martin, 2017) is available at
727 http://fizz.phys.dal.ca/~atmos/martin/?page_id=1520. A database of atmospheric N_r
728 concentration and deposition from the nationwide monitoring network in China is
729 available at <https://www.nature.com/articles/s41597-019-0061-2>. Measured N_r
730 concentration and deposition datasets in the United States are available on the website:
731 <https://www.epa.gov/outdoor-air-quality-data>. Measured surface NO₂ and NH₃
732 concentration datasets in Europe are available at
733 <https://www.nilu.no/projects/ccc/emepdata.html>. Global surface NO₂ and NH₃
734 concentration data used to calculate the longterm trends in **Fig. 13** and **Fig. 14** have
735 been released on the website: <https://zenodo.org/record/3546517#.Xj6I4GgzY2w>.

736 **Competing interests.** The authors declare no competing financial interests.

737 **Reference**

738 Amos, H. M., Jacob, D. J., Holmes, C. D., Fisher, J. A., Wang, Q., Yantosca, R. M.,

739 Corbitt, E. S., Galarneau, E., Rutter, A. P., and Gustin, M. S.: Gas-particle partitioning

740 of atmospheric Hg(II) and its effect on global mercury deposition, *Atmos. Chem.*

741 *Phys.*, 11, 29441-29477, 2012.

742 Beer, R., Shephard, M. W., Kulawik, S. S., Clough, S. A., Eldering, A., Bowman, K.

743 W., Sander, S. P., Fisher, B. M., Payne, V. H., Luo, M., Osterman, G. B., and Worden,

744 J. R.: First satellite observations of lower tropospheric ammonia and methanol,

745 *Geophys. Res Lett.*, 35, 1-5, 10.1029/2008GL033642, 2008.

746 Bobbink, R., Hicks, K., Galloway, J., Spranger, T., Alkemade, R., Ashmore, M.,

747 Bustamante, M., Cinderby, S., Davidson, E., Dentener, F., Emmett, B., Erisman, J.-W.,

748 Fenn, M., Gilliam, F., Nordin, A., Pardo, L., and De Vries, W.: Global assessment of

749 nitrogen deposition effects on terrestrial plant diversity: a synthesis, *Ecological*

750 *Applications*, 20, 30-59, doi:10.1890/08-1140.1, 2010.

751 Boersma, K. F., Eskes, H. J., Dirksen, R. J., van der A, R. J., Veefkind, J. P., Stammes,

752 P., Huijnen, V., Kleipool, Q. L., Sneep, M., Claas, J., Leitão, J., Richter, A., Zhou, Y.,

753 and Brunner, D.: An improved tropospheric NO₂ column retrieval algorithm for the

754 Ozone Monitoring Instrument, *Atmospheric Measurement Techniques*, 4, 1905-1928,

755 10.5194/amt-4-1905-2011, 2011.

756 Canfield, D. E., Glazer, A. N., and Falkowski, P. G.: The evolution and future of

757 Earth's nitrogen cycle, *Science*, 330, 192-196, 2010.

758 Cao, G. L., Zhang, X. Y., and Gong, S. L.: Emission inventories of primary particles
759 and pollutant gases for China, *Science Bulletin*, 56, 781-788, 2011.

760 Cheng, M., Jiang, H., Guo, Z., Zhang, X., and Lu, X.: Estimating NO₂ dry deposition
761 using satellite data in eastern China, *Int. J. Remote Sens.*, 34, 2548-2565, 2013.

762 Coheur, P.-F., Clarisse, L., Turquety, S., Hurtmans, D., and Clerbaux, C.: IASI
763 measurements of reactive trace species in biomass burning plumes, *Atmos. Chem.*
764 *Phys.*, 9, 5655-5667, 2009.

765 Crippa, M., Guizzardi, D., Muntean, M., Schaaf, E., Dentener, F., van Aardenne, J. A.,
766 Monni, S., Doering, U., Olivier, J. G. J., Pagliari, V., and Janssens-Maenhout, G.:
767 Gridded emissions of air pollutants for the period 1970–2012 within EDGAR v4.3.2,
768 *Earth Syst. Sci. Data*, 10, 1987-2013, 10.5194/essd-10-1987-2018, 2018.

769 Dammers, E., Palm, M., Van Damme, M., Vigouroux, C., Smale, D., Conway, S.,
770 Toon, G. C., Jones, N., Nussbaumer, E., Warneke, T., Petri, C., Clarisse, L., Clerbaux,
771 C., Hermans, C., Lutsch, E., Strong, K., Hannigan, J. W., Nakajima, H., Morino, I.,
772 Herrera, B., Stremme, W., Grutter, M., Schaap, M., Wichink Kruit, R. J., Notholt, J.,
773 Coheur, P. F., and Erisman, J. W.: An evaluation of IASI-NH₃ with ground-based
774 Fourier transform infrared spectroscopy measurements, *Atmos. Chem. Phys.*, 16,
775 10351-10368, 10.5194/acp-16-10351-2016, 2016.

776 David, F., M, C., U, S., MA, S., JN, C., S, R., LJ, S., A, J., B, G., and JN, G.: The
777 global nitrogen cycle in the twenty-first century, *Philosophical Transactions of the*
778 *Royal Society of London*, 368, 20130164, 2013.

779 Emmons, L., Walters, S., Hess, P., Lamarque, J.-F., Pfister, G., Fillmore, D., Granier,

780 C., Guenther, A., Kinnison, D., and Laepple, T.: Description and evaluation of the
781 Model for Ozone and Related chemical Tracers, version 4 (MOZART-4),
782 Geoscientific Model Development, 3, 43-67, 2010.

783 Erisman, J. W., Sutton, M. A., Galloway, J., Klimont, Z., and Winiwarter, W.: How a
784 century of ammonia synthesis changed the world, Nat. Geosci., 1, 636-639, 2008.

785 Farquhar, G. D., Firth, P. M., Wetselaar, R., and Weir, B.: On the Gaseous Exchange
786 of Ammonia between Leaves and the Environment: Determination of the Ammonia
787 Compensation Point, Plant Physiology, 66, 710-714, 10.1104/pp.66.4.710, 1980.

788 Galloway, J. N., Dentener, F. J., Capone, D. G., Boyer, E. W., Howarth, R. W.,
789 Seitzinger, S. P., Asner, G. P., Cleveland, C., Green, P., and Holland, E.: Nitrogen
790 cycles: past, present, and future, Biogeochemistry, 70, 153-226, 2004a.

791 Galloway, J. N., Dentener, F. J., Capone, D. G., Boyer, E. W., Howarth, R. W.,
792 Seitzinger, S. P., Asner, G. P., Cleveland, C. C., Green, P. A., Holland, E. A., Karl, D.
793 M., Michaels, A. F., Porter, J. H., Townsend, A. R., and Vösmarty, C. J.: Nitrogen
794 Cycles: Past, Present, and Future, Biogeochemistry, 70, 153-226,
795 10.1007/s10533-004-0370-0, 2004b.

796 Galloway, J. N., Townsend, A. R., Erisman, J. W., Bekunda, M., Cai, Z., Freney, J. R.,
797 Martinelli, L. A., Seitzinger, S. P., and Sutton, M. A.: Transformation of the nitrogen
798 cycle: recent trends, questions, and potential solutions, Science, 320, 889-892, 2008.

799 Geddes, J. A., Martin, R. V., Boys, B. L., and van Donkelaar, A.: Long-term trends
800 worldwide in ambient NO₂ concentrations inferred from satellite observations,
801 Environmental Health Perspectives, 124, 281, 2016.

802 Geddes, J. A., and Martin, R. V.: Global deposition of total reactive nitrogen oxides
803 from 1996 to 2014 constrained with satellite observations of NO₂ columns, *Atmos.*
804 *Chem. Phys.*, 17, 10071-10091, 2017.

805 Graaf, S. C. v. d., Dammers, E., Schaap, M., and Erisman, J. W.: How are NH₃ dry
806 deposition estimates affected by combining the LOTOS-EUROS model with
807 IASI-NH₃ satellite observations?, *Atmos. Chem. Phys.*, 18, 13173-13196,
808 <https://doi.org/10.5194/acp-2018-133>, 2018.

809 Grell, G. A., Peckham, S. E., Schmitz, R., McKeen, S. A., Frost, G., Skamarock, W.
810 C., and Eder, B.: Fully coupled “online” chemistry within the WRF model, *Atmos.*
811 *Environ.*, 39, 6957-6975, 2005.

812 Hoesly, R. M., Smith, S. J., Feng, L., Klimont, Z., Janssens-Maenhout, G., Pitkanen,
813 T., Seibert, J. J., Vu, L., Andres, R. J., Bolt, R. M., Bond, T. C., Dawidowski, L.,
814 Kholod, N., Kurokawa, J. I., Li, M., Liu, L., Lu, Z., Moura, M. C. P., O'Rourke, P. R.,
815 and Zhang, Q.: Historical (1750–2014) anthropogenic emissions of reactive gases and
816 aerosols from the Community Emissions Data System (CEDS), *Geosci. Model Dev.*,
817 11, 369-408, [10.5194/gmd-11-369-2018](https://doi.org/10.5194/gmd-11-369-2018), 2018.

818 Janssens, I. A., Dieleman, W., Luysaert, S., Subke, J. A., Reichstein, M., Ceulemans,
819 R., Ciais, P., Dolman, A. J., Grace, J., Matteucci, G., Papale, D., Piao, S. L., Schulze,
820 E. D., Tang, J., and Law, B. E.: Reduction of forest soil respiration in response to
821 nitrogen deposition, *Nat. Geosci.*, 3, 315, [10.1038/ngeo844](https://doi.org/10.1038/ngeo844)
822 <https://www.nature.com/articles/ngeo844#supplementary-information>, 2010.

823 Jia, Y., Yu, G., Gao, Y., He, N., Wang, Q., Jiao, C., and Zuo, Y.: Global inorganic

824 nitrogen dry deposition inferred from ground-and space-based measurements,
825 Scientific reports, 6, 1-11, 2016.

826 Kharol, S. K., Martin, R. V., Philip, S., Boys, B., Lamsal, L. N., Jerrett, M., Brauer,
827 M., Crouse, D. L., Mclinden, C., and Burnett, R. T.: Assessment of the magnitude and
828 recent trends in satellite-derived ground-level nitrogen dioxide over North America,
829 Atmos. Environ., 118, 236-245, 2015.

830 Kharol, S. K., Shephard, M. W., McLinden, C. A., Zhang, L., Sioris, C. E., O'Brien, J.
831 M., Vet, R., Cady-Pereira, K. E., Hare, E., Siemons, J., and Krotkov, N. A.: Dry
832 Deposition of Reactive Nitrogen From Satellite Observations of Ammonia and
833 Nitrogen Dioxide Over North America, Geophys. Res Lett., 45, 1157-1166,
834 10.1002/2017GL075832, 2018.

835 Kim, T. W., Lee, K., Duce, R., and Liss, P.: Impact of atmospheric nitrogen deposition
836 on phytoplankton productivity in the South China Sea, Geophys. Res Lett., 41, 3156–
837 3162, 2014.

838 Kuik, F., Lauer, A., Churkina, G., Denier van der Gon, H. A. C., Fenner, D., Mar, K.
839 A., and Butler, T. M.: Air quality modelling in the Berlin-Brandenburg region using
840 WRF-Chem v3.7.1: sensitivity to resolution of model grid and input data,
841 Geoscientific Model Development Discussions, 9, 4339-4363, 2016.

842 Lamarque, J. F., Kiehl, J., Brasseur, G., Butler, T., Cameron - Smith, P., Collins, W.,
843 Collins, W., Granier, C., Hauglustaine, D., and Hess, P.: Assessing future nitrogen
844 deposition and carbon cycle feedback using a multimodel approach: Analysis of
845 nitrogen deposition, Journal of Geophysical Research: Atmospheres (1984–2012), 110,

846 2005.

847 Lamsal, L. N., Martin, R. V., van Donkelaar, A., Steinbacher, M., Celarier, E. A.,
848 Bucsela, E., Dunlea, E. J., and Pinto, J. P.: Ground-level nitrogen dioxide
849 concentrations inferred from the satellite-borne Ozone Monitoring Instrument, *J.*
850 *Geophys. Res-Atmos.*, 113, 1-15, 10.1029/2007JD009235, 2008.

851 Lamsal, L. N., Martin, R. V., Parrish, D. D., and Krotkov, N. A.: Scaling relationship
852 for NO₂ pollution and urban population size: a satellite perspective, *Environ. Sci.*
853 *Technol.*, 47, 7855-7861, 2013.

854 Larkin, A., Geddes, J. A., Martin, R. V., Xiao, Q., Liu, Y., Marshall, J. D., Brauer, M.,
855 and Hystad, P.: Global Land Use Regression Model for Nitrogen Dioxide Air
856 Pollution, *Environ. Sci. Technol.*, 51, 6957-6964, 2017.

857 Larssen, T., Duan, L., and Mulder, J.: Deposition and leaching of sulfur, nitrogen and
858 calcium in four forested catchments in China: implications for acidification, *Environ.*
859 *Sci. Technol.*, 45, 1192-1198, 2011.

860 Levine, S. Z., and Schwartz, S. E.: In-cloud and below-cloud scavenging of Nitric
861 acid vapor, *Atmospheric Environment* (1967), 16, 1725-1734,
862 [https://doi.org/10.1016/0004-6981\(82\)90266-9](https://doi.org/10.1016/0004-6981(82)90266-9), 1982.

863 Li, Y., Thompson, T. M., Damme, M. V., Chen, X., Benedict, K. B., Shao, Y., Day, D.,
864 Boris, A., Sullivan, A. P., and Ham, J.: Temporal and Spatial Variability of Ammonia
865 in Urban and Agricultural Regions of Northern Colorado, United States, *Atmos. Chem.*
866 *Phys.*, 17, 1-50, 2017.

867 Liu, H., Jacob, D. J., Bey, I., and Yantosca, R. M.: Constraints from ²¹⁰Pb and ⁷Be on

868 wet deposition and transport in a global three-dimensional chemical tracer model
869 driven by assimilated meteorological fields, *J. Geophys. Res-Atmos.*, 106,
870 12109-12128, 10.1029/2000JD900839, 2001.

871 Liu, L., Zhang, X., Xu, W., Liu, X., Lu, X., Chen, D., Zhang, X., Wang, S., and Zhang,
872 W.: Estimation of monthly bulk nitrate deposition in China based on satellite NO₂
873 measurement by the Ozone Monitoring Instrument, *Remote Sens. Environ.*, 199,
874 93-106, 2017a.

875 Liu, L., Zhang, X., Xu, W., Liu, X., Lu, X., Wang, S., Zhang, W., and Zhao, L.:
876 Ground Ammonia Concentrations over China Derived from Satellite and Atmospheric
877 Transport Modeling, *Remote Sens.*, 9, 467, 2017b.

878 Liu, L., Zhang, X., Zhang, Y., Xu, W., Liu, X., Zhang, X., Feng, J., Chen, X., Zhang,
879 Y., Lu, X., Wang, S., Zhang, W., and Zhao, L.: Dry Particulate Nitrate Deposition in
880 China, *Environ. Sci. Technol.*, 51, 5572-5581, 10.1021/acs.est.7b00898, 2017c.

881 Liu, L., Zhang, X., Wong, A. Y. H., Xu, W., Liu, X., Li, Y., Mi, H., Lu, X., Zhao, L.,
882 Wang, Z., and Wu, X.: Estimating global surface ammonia concentrations inferred
883 from satellite retrievals, *Atmos. Chem. Phys.*, 19, 12051-12066,
884 10.5194/acp-2019-184, 2019.

885 Liu, L., Zhang, X., Xu, W., Liu, X., Wei, J., Wang, Z., and Yang, Y.: Global estimates
886 of dry ammonia deposition inferred from space-measurements, *Sci.Total Environ.*,
887 730, 139189, <https://doi.org/10.1016/j.scitotenv.2020.139189>, 2020.

888 Liu, X., Duan, L., Mo, J., Du, E., Shen, J., Lu, X., Zhang, Y., Zhou, X., He, C., and
889 Zhang, F.: Nitrogen deposition and its ecological impact in China: An overview,

890 Environ. Pollut., 159, 2251-2264, <http://dx.doi.org/10.1016/j.envpol.2010.08.002>,
891 2011.

892 Liu, X., Xu, W., Duan, L., Du, E., Pan, Y., Lu, X., Zhang, L., Wu, Z., Wang, X.,
893 Zhang, Y., Shen, J., Song, L., Feng, Z., Liu, X., Song, W., Tang, A., Zhang, Y., Zhang,
894 X., and Collett, J. L.: Atmospheric Nitrogen Emission, Deposition, and Air Quality
895 Impacts in China: an Overview, Curr. Pollut. Rep., 3, 65-77,
896 10.1007/s40726-017-0053-9, 2017d.

897 Lu, X., Jiang, H., Zhang, X., Liu, J., Zhang, Z., Jin, J., Wang, Y., Xu, J., and Cheng,
898 M.: Estimated global nitrogen deposition using NO₂ column density, Int. J. Remote
899 Sens., 34, 8893-8906, 2013.

900 Mari, C., Jacob, D. J., and Bechtold, P.: Transport and scavenging of soluble gases in
901 a deep convective cloud, J. Geophys. Res-Atmos., 105, 22255-22268, 2000.

902 Nadelhoffer, K. J., Emmett, B. A., Gundersen, P., Kjønaas, O. J., Koopmans, C. J.,
903 Schlegel, P., Tietema, A., and Wright, R. F.: Nitrogen deposition makes a minor
904 contribution to carbon sequestration in temperate forests, Nature, 398, 145,
905 10.1038/18205, 1999.

906 Nemitz, E., Flynn, M., Williams, P. I., Milford, C., Theobald, M. R., Blatter, A.,
907 Gallagher, M. W., and Sutton, M. A.: A Relaxed Eddy Accumulation System for the
908 Automated Measurement of Atmospheric Ammonia Fluxes, Water, Air and Soil
909 Pollution: Focus, 1, 189-202, 10.1023/A:1013103122226, 2001.

910 Nicolas, G., and Galloway, J. N.: An Earth-system perspective of the global nitrogen
911 cycle, Nature, 451, 293-296, 2008.

912 Nowlan, C., Martin, R., Philip, S., Lamsal, L., Krotkov, N., Marais, E., Wang, S., and
913 Zhang, Q.: Global dry deposition of nitrogen dioxide and sulfur dioxide inferred from
914 space-based measurements, *Global Biogeochem. Cy.*, 28, 1025-1043, 2014.

915 Paerl, H. W., Gardner, W. S., Mccarthy, M. J., Peierls, B. L., and Wilhelm, S. W.:
916 Algal blooms: noteworthy nitrogen, *Science*, 346, 175, 2014.

917 Pan, Y., Wang, Y., Tang, G., and Wu, D.: Wet and dry deposition of atmospheric
918 nitrogen at ten sites in Northern China, *Atmos. Chem. Phys.*, 12, 6515-6535, 2012.

919 Ronsmans, G., Langerock, B., Wespes, C., Hannigan, J. W., Hase, F., Kerzenmacher,
920 T., Mahieu, E., Schneider, M., Smale, D., Hurtmans, D., De Mazi ère, M., Clerbaux, C.,
921 and Coheur, P. F.: First characterization and validation of FORLI-HNO₃ vertical
922 profiles retrieved from IASI/Metop, *Atmos. Meas. Tech.*, 9, 4783-4801,
923 10.5194/amt-9-4783-2016, 2016.

924 Schrader, F., Brümmer, C., Flechard, C. R., Wichink Kruit, R. J., van Zanten, M. C.,
925 Zöll, U., Hensen, A., and Erisman, J. W.: Non-stomatal exchange in ammonia dry
926 deposition models: comparison of two state-of-the-art approaches, *Atmos. Chem.*
927 *Phys.*, 16, 13417-13430, 10.5194/acp-16-13417-2016, 2016.

928 Shen, J., Li, Y., Liu, X., Luo, X., Tang, H., Zhang, Y., and Wu, J.: Atmospheric dry
929 and wet nitrogen deposition on three contrasting land use types of an agricultural
930 catchment in subtropical central China, *Atmos. Environ.*, 67, 415-424,
931 <http://dx.doi.org/10.1016/j.atmosenv.2012.10.068>, 2013.

932 Stevens, C. J., Dise, N. B., Mountford, J. O., and Gowing, D. J.: Impact of Nitrogen
933 Deposition on the Species Richness of Grasslands, *Science*, 303, 1876-1879,

934 10.1126/science.1094678, 2004.

935 Sutton, M. A., Tang, Y. S., Miners, B., and Fowler, D.: A New Diffusion Denuder
936 System for Long-Term, Regional Monitoring of Atmospheric Ammonia and
937 Ammonium, *Water Air & Soil Pollution Focus*, 1, 145-156, 2001.

938 Sutton, M. A., Bleeker, A., Howard, C. M., Bekunda, M., Grizzetti, B., Vries, W. D.,
939 Grinsven, H. J. M. V., Abrol, Y. P., Adhya, T. K., and Billen, G.: Our Nutrient World:
940 the challenge to produce more food and energy with less pollution, 2013.

941 Tan, J., Fu, J. S., Dentener, F., Sun, J., Emmons, L., Tilmes, S., Sudo, K., Flemming,
942 J., Jonson, J. E., and Gravel, S.: Multi-model study of HTAP II on sulfur and nitrogen
943 deposition, *Atmos. Chem. Phys.*, 18, 1-36, 2018.

944 Van Damme, M., Clarisse, L., Dammers, E., Liu, X., Nowak, J., Clerbaux, C.,
945 Flechard, C., Galy-Lacaux, C., Xu, W., and Neuman, J.: Towards validation of
946 ammonia (NH₃) measurements from the IASI satellite, *Atmospheric Measurement
947 Techniques*, 7, 12125-12172, 2014a.

948 Van Damme, M., Wichink Kruit, R., Schaap, M., Clarisse, L., Clerbaux, C., Coheur, P.
949 F., Dammers, E., Dolman, A., and Erisman, J.: Evaluating 4 years of atmospheric
950 ammonia (NH₃) over Europe using IASI satellite observations and LOTOS-EUROS
951 model results, *J. Geophys. Res-Atmos.*, 119, 9549-9566, 2014b.

952 Van der Graaf, S. C., Dammers, E., Schaap, M., and Erisman, J. W.: Technical note:
953 How are NH₃ dry deposition estimates affected by combining the LOTOS-EUROS
954 model with IASI-NH₃ satellite observations?, *Atmos. Chem. Phys.*, 18, 13173-13196,
955 10.5194/acp-18-13173-2018, 2018.

956 Vet, R., Artz, R. S., Carou, S., Shaw, M., Ro, C.-U., Aas, W., Baker, A., Bowersox, V.
957 C., Dentener, F., Galy-Lacaux, C., Hou, A., Pienaar, J. J., Gillett, R., Forti, M. C.,
958 Gromov, S., Hara, H., Khodzher, T., Mahowald, N. M., Nickovic, S., Rao, P. S. P., and
959 Reid, N. W.: A global assessment of precipitation chemistry and deposition of sulfur,
960 nitrogen, sea salt, base cations, organic acids, acidity and pH, and phosphorus, *Atmos.*
961 *Environ.*, 93, 3-100, <http://dx.doi.org/10.1016/j.atmosenv.2013.10.060>, 2014.

962 Vitousek, P. M., Aber, J. D., Howarth, R. W., Likens, G. E., Matson, P. A., Schindler,
963 D. W., Schlesinger, W. H., and Tilman, D. G.: Human alteration of the global nitrogen
964 cycle: sources and consequences, *Ecol. Appl.*, 7, 737-750, 1997.

965 Wesely, M., and Hicks, B.: Some factors that affect the deposition rates of sulfur
966 dioxide and similar gases on vegetation, *Journal of the Air Pollution Control*
967 *Association*, 27, 1110-1116, 1977.

968 Whitburn, S., Van Damme, M., Clarisse, L., Bauduin, S., Heald, C. L., Hadji-Lazaro,
969 J., Hurtmans, D., Zondlo, M. A., Clerbaux, C., and Coheur, P. F.: A flexible and robust
970 neural network IASI-NH₃ retrieval algorithm, *J. Geophys. Res-Atmos.*, 121,
971 6581-6599, 10.1002/2016JD024828, 2016.

972 Williams, J. E., Boersma, K. F., Le Sager, P., and Verstraeten, W. W.: The
973 high-resolution version of TM5-MP for optimized satellite retrievals: description and
974 validation, *Geosci. Model Dev.*, 10, 721-750, 10.5194/gmd-10-721-2017, 2017.

975 Wong, D. C., Pleim, J., Mathur, R., Binkowski, F., Otte, T., Gilliam, R., Pouliot, G.,
976 Xiu, A., Young, J. O., and Kang, D.: WRF-CMAQ two-way coupled system with
977 aerosol feedback: software development and preliminary results, *Geosci. Model Dev.*,

978 5, 299-312, 10.5194/gmd-5-299-2012, 2012.

979 Xu, W., Luo, X. S., Pan, Y. P., Zhang, L., Tang, A. H., Shen, J. L., Zhang, Y., Li, K. H.,
980 Wu, Q. H., Yang, D. W., Zhang, Y. Y., Xue, J., Li, W. Q., Li, Q. Q., Tang, L., Lv, S. H.,
981 Liang, T., Tong, Y. A., Liu, P., Zhang, Q., Xiong, Z. Q., Shi, X. J., Wu, L. H., Shi, W.
982 Q., Tian, K., Zhong, X. H., Shi, K., Tang, Q. Y., Zhang, L. J., Huang, J. L., He, C. E.,
983 Kuang, F. H., Zhu, B., Liu, H., Jin, X., Xin, Y. J., SHi, X. K., Du, E. Z., Dore, A. J.,
984 Tang, S., Collett Jr, J. L., Goulding, K., Sun, Y. X., Ren, J., Zhang, F. S., and Liu, X. J.:
985 Quantifying atmospheric nitrogen deposition through a nationwide monitoring
986 network across China, *Atmos. Chem. Phys.*, 15, 12345-12360, 2015.

987 Yu, G., Jia, Y., He, N., Zhu, J., Chen, Z., Wang, Q., Piao, S., Liu, X., He, H., Guo, X.,
988 Wen, Z., Li, P., Ding, G., and Goulding, K.: Stabilization of atmospheric nitrogen
989 deposition in China over the past decade, *Nat. Geosci.*, 12, 424-429,
990 10.1038/s41561-019-0352-4, 2019.

991 Zhang, L., Wright, L. P., and Asman, W. A. H.: Bi-directional air-surface exchange of
992 atmospheric ammonia: A review of measurements and a development of a big-leaf
993 model for applications in regional-scale air-quality models, *J. Geophys. Res-Atmos.*,
994 115, 898-907, 2010.

995 Zhang, L., Jacob, D. J., Knipping, E. M., Kumar, N., Munger, J. W., Carouge, C., Van
996 Donkelaar, A., Wang, Y., and Chen, D.: Nitrogen deposition to the United States:
997 distribution, sources, and processes, *Atmos. Chem. Phys.*, 12 4539-4554, 2012.

998 Zhang, Q., Streets, D. G., Carmichael, G. R., He, K., Huo, H., Kannari, A., Klimont,
999 Z., Park, I., Reddy, S., and Fu, J.: Asian emissions in 2006 for the NASA INTEX-B

1000 mission, *Atmos. Chem. Phys.*, 9, 5131-5153, 2009.

1001 Zhang, X. Y., Lu, X. H., Liu, L., Chen, D. M., Zhang, X. M., Liu, X. J., and Zhang, Y.:
1002 Dry deposition of NO₂ over China inferred from OMI columnar NO₂ and atmospheric
1003 chemistry transport model, *Atmos. Environ.*, 169, 2017.

1004 Zhang, X. Y., Chuai, X. W., Liu, L., Zhang, W. T., Lu, X. H., Zhao, L. M., and Chen,
1005 D. M.: Decadal Trends in Wet Sulfur Deposition in China Estimated From OMI SO₂
1006 Columns, *J. Geophys. Res-Atmos.*, 123, 10796-10811, 10.1029/2018JD028770, 2018.

1007 Zhao, X., Chen, L., and Zhang, H.: Nitrate and ammonia contaminations in drinking
1008 water and the affecting factors in Hailun, northeast China, *Journal of Environmental*
1009 *Health*, 75, 28, 2013.

1010 Zhao, Y., Zhang, L., Chen, Y., Liu, X., Xu, W., Pan, Y., and Duan, L.: Atmospheric
1011 nitrogen deposition to China: A model analysis on nitrogen budget and critical load
1012 exceedance, *Atmos. Environ.*, 153, 32-40,
1013 <http://dx.doi.org/10.1016/j.atmosenv.2017.01.018>, 2017.

1014